



Communication

Impact of Sapphire Step Height on the Growth of Monolayer Molybdenum Disulfide

Jie Lu ^{1,†}, Miaomiao Zheng ^{1,†}, Jinxin Liu ¹, Yufeng Zhang ¹ , Xueao Zhang ^{1,2,*} and Weiwei Cai ^{1,2,*}

¹ College of Physical Science and Technology, Xiamen University, Xiamen 361005, China; 19820190154689@stu.xmu.edu.cn (J.L.); zhengmiaomiao@stu.xmu.edu.cn (M.Z.); jxliu@stu.xmu.edu.cn (J.L.); yufengzhang@xmu.edu.cn (Y.Z.)

² Jiujiang Research Institute, Xiamen University, Jiujiang 360404, China

* Correspondence: xazhang@xmu.edu.cn (X.Z.); wwcai@xmu.edu.cn (W.C.)

† These authors contributed equally to this work.

Abstract: Although the synthesis of molybdenum disulfide (MoS₂) on sapphire has made a lot of progress, how the substrate surface affects the growth still needs to be further studied. Herein, the impact of the sapphire step height on the growth of monolayer MoS₂ through chemical vapor deposition (CVD) is studied. The results show that MoS₂ exhibits a highly oriented triangular grain on a low-step (0.44–1.54 nm) substrate but nanoribbons with a consistent orientation on a high-step (1.98–3.30 nm) substrate. Triangular grains exhibit cross-step growth, with one edge parallel to the step edge, while nanoribbons do not cross steps and possess the same orientation as the step. Scanning electron microscopy (SEM) reveals that nanoribbons are formed by splicing multiple grains, and the consistency of the orientation of these grains is demonstrated with a transmission electron microscope (TEM) and second-harmonic generation (SHG). Furthermore, our CP2K calculations, conducted using the generalized gradient approximation and the Perdew–Burke–Ernzerhof (PBE) functional with D3 (BJ) correction, show that MoS₂ domains prefer to nucleate at higher steps, while climbing across a higher step is more difficult. This work not only sheds light on the growth mechanism of monolayer MoS₂ but also promotes its applications in electrical, optical, and energy-related devices.

Keywords: chemical vapor deposition; monolayer MoS₂; morphology; sapphire step height



Citation: Lu, J.; Zheng, M.; Liu, J.; Zhang, Y.; Zhang, X.; Cai, W. Impact of Sapphire Step Height on the Growth of Monolayer Molybdenum Disulfide. *Nanomaterials* **2023**, *13*, 3056. <https://doi.org/10.3390/nano13233056>

Academic Editor: Silvia Villar-Rodil

Received: 25 October 2023

Revised: 21 November 2023

Accepted: 27 November 2023

Published: 30 November 2023



Copyright: © 2023 by the authors. Licensee MDPI, Basel, Switzerland. This article is an open access article distributed under the terms and conditions of the Creative Commons Attribution (CC BY) license (<https://creativecommons.org/licenses/by/4.0/>).

1. Introduction

Molybdenum disulfide (MoS₂) has garnered great attention due to its immense potential in various applications, such as transistors, photodetectors, and catalysis [1–4]. The preparation of MoS₂ is crucial for achieving these applications. The simulation works reveal that the role of substrates, capping layers, etc., is significant to the growth of MoS₂ and related materials, which guides experimental works [5–7]. Currently, two types of substrates are generally used in synthesis: amorphous and single-crystal. The former is represented by silica and glass [8,9]. The crystal orientation is disordered when growing on these substrates, which results in polycrystalline films. The latter is represented by sapphire, mica, and single-crystal gold [10–12]. The crystals exhibit van der Waals epitaxy, with specific orientations on the surface of such substrates and suitable growth conditions. This is beneficial for the controllable synthesis of MoS₂, so this type of substrate has become a preferred choice. Among them, the growth of MoS₂ on sapphire is widely studied. Firstly, as an industrial product, sapphire is easy to obtain and inexpensive. Secondly, C-plane sapphire possesses a six-fold symmetric structure, which matches the three-fold symmetry of MoS₂, making epitaxial growth more likely to occur. Furthermore, sapphire substrates can be polished and annealed to form surfaces with low roughness, which is very beneficial for material growth and transfer. In addition, the lattice constant and in-plane expansion coefficient of sapphire are greater than those of MoS₂, which ensures that the material is always stretched on the substrate surface and does not develop wrinkles. Therefore,

studying the growth behavior of MoS₂ on sapphire substrates is of great significance for the preparation and application development of MoS₂.

The surface of sapphire can generate steps after annealing, which have a significant impact on the growth of MoS₂. Li et al. and Wang et al. prepared wafer-scale MoS₂ single crystals by designing the step direction of the substrate [13,14]. Subsequently, Zheng et al. discovered that the immature steps promote grain nucleation near the step edges and guide the unidirectional alignment regardless of the step direction [15]. Furthermore, Liu et al. found that steps with a height of about 1.26 nm can induce the nucleation of double-layer MoS₂ [16]. In addition, the theoretical calculations indicated that different step heights regulate the nucleation of MoS₂ with different layer thicknesses, providing insights for the preparation of multi-layer materials [17].

Here, we utilized different annealing processes to obtain low-step (0.44–1.54 nm) sapphire substrates (LSSs) and high-step (1.98–3.30 nm) sapphire substrates (HSSs). Unidirectional MoS₂ triangle grains and nanoribbons were achieved on LSS and HSS, respectively. Nanoribbons were formed with multiple grains, and the single-crystal nature of the nanoribbons was demonstrated through TEM and SHG measurements. Theoretical calculations conducted using CP2K suggest that the high steps promote the nucleation of monolayer MoS₂ and prevent cross-step growth. This work sheds light on the growth of monolayer MoS₂ and its potential in various applications.

2. Materials and Methods

2.1. Annealing of Sapphire

We chose c-plane sapphire (HeFei crystal Technical Material, Hefei, China) with a miscut angle of ~1° towards the A-axis (C/A) as the substrate. Before the growth, the substrates were annealed under atmospheric pressure to generate steps on the surface. Low-step (0.44–1.54 nm) sapphire substrates (LSS) were obtained through annealing at 1000 °C for 3 h and then cooling to room temperature at a rate of 10 °C/min, while high-step (1.98–3.30 nm) sapphire substrates (HSS) were produced through annealing at 1100 °C for 3 h and naturally cooling to room temperature.

2.2. Synthesis of MoS₂

The growth of MoS₂ was performed in a low-pressure (150 Pa) CVD system (Anhui BEQ Equipment Technology, Hefei, China). S powder (purchased from Alfa, 99.995%, 10 g) was loaded in the main tube and carried by 100 SCCM Ar, while MoO₃ powder (Alfa, 99.95%, 20 mg) was loaded in the tiny tube and carried by 50 SCCM Ar. A piece of annealed sapphire was placed downstream as the substrate. The temperature of S, MoO₃, and the substrate was 200 °C, 580 °C, and 850 °C, respectively. The growth duration was maintained at 15 min, and then the furnace was naturally cooled to room temperature.

2.3. Sample Characterizations

The morphology of the MoS₂ samples was obtained with an optical microscope (OM, BX51M, Olympus, Tokyo, Japan), a scanning electron microscope (SEM, Sigma HD, Zeiss, Oberkochen, Germany), and an atomic force microscope (AFM, ICON, Bruker, Billerica, MA, USA). Raman, photoluminescence (PL), and second-harmonic generation (SHG) were recorded on a confocal laser microscope system (Alpha 300RS+, WITec, Ulm, Germany). Selected-area electron diffraction (SAED) patterns and high-resolution TEM (HRTEM) images were obtained via a transmission electron microscope (TEM, F200S G2, Thermo Fisher, Waltham, MA, USA).

2.4. CP2K Calculation

All calculations were performed with periodic DFT using the Gaussian and Plane Wave (GPW) method implemented in CP2K's Quickstep module (2023, version 2023.1; the CP2K developers group) [18,19]. The explorative studies of these structures were performed using the molecularly optimized basis set DZVP-MOLOPT-SR-GTH for each

atom with a Goedecker–Teter–Hutter (GTH) pseudopotential [20–22]. The calculations were conducted using the generalized gradient approximation and the Perdew–Burke–Ernzerhof (PBE) functional [23] with D3 (BJ) correction [24]. The orbital transformation method was used to converge the self-consistent field (SCF) cycle with an electronic gradient tolerance value of 5×10^{-6} Hartree. An energy cutoff of 350 Ry was used throughout the calculations. Vacuum spacing larger than 15 Å was introduced to avoid artificial interaction between the periodic images along the z-direction. The input file was generated with Multiwfn software (2023, Multiwfn version 3.8(dev), Beijing Kein Research Center for Natural Sciences, Beijing, China) [25].

3. Results and Discussion

An LSS and HSS were used for the substrate to investigate the effect of step height on the growth of monolayer MoS₂. Figure 1a,e illustrate the step height distribution of the LSS and the HSS, respectively. It is observed that, on the LSS, the step height ranges from 0.44 to 1.54 nm and is concentrated at 1.10 nm, whereas the steps on the HSS are quite steep, and its height distribution is more extensive (1.98–3.30 nm). An optical microscopy (OM) image of the MoS₂ grains grown on the LSS (Figure 1b) shows a typical triangle shape with a uniform orientation. In contrast, the MoS₂ grains grown on the HSS (Figure 1f) exhibit a nanoribbon shape with a uniform orientation. The detailed morphology of the two types of grains was characterized through AFM. As shown in Figure 1c,g, the thickness of the triangle and nanoribbon grains is 0.68 and 0.72 nm, respectively, indicating that both grains are monolayer. The triangle grains grow across the step, and one side of the grain is parallel to the edge of the step, which is consistent with the result of the literature [13]. However, the growth of the MoS₂ nanoribbons ceases at the edge of the step, and the nanoribbons share the same direction with steps. As shown in Figure 1d,h, the Raman spectra of the MoS₂ grown on different steps show two peaks, E_{2g} (~386 cm⁻¹) and A_{1g} (~405 cm⁻¹), with a peak position difference of ~19 cm⁻¹. No noticeable differences in the peak position, full width at half maxima (FWHM), and intensity are observed, indicating that the step height does not affect the quality of MoS₂. Moreover, the PL spectra of these two types of MoS₂ are consistent in Figure S1, which confirms the above conclusion.

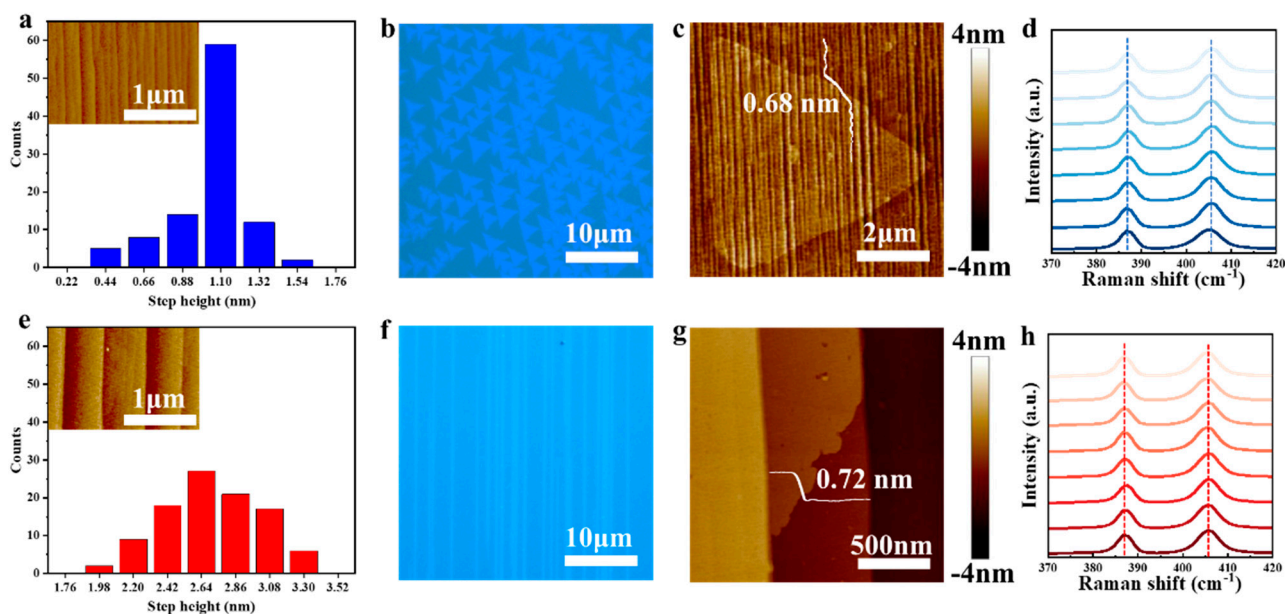


Figure 1. Step height distribution and the growth results of monolayer MoS₂ on LSS and HSS. Statistics on the step height of LSS (a) and HSS (e). OM images of MoS₂ on LSS (b) and HSS (f). AFM images of MoS₂ grown on LSS (c) and HSS (g). Raman spectrum of MoS₂ on LSS (d) and HSS (h).

SEM was performed to investigate the evolution of the morphology of the nanoribbons over the deposition time. As shown in Figure 2a, scattered grains form on the substrate surface when the growth lasts for 5 min. If the deposition time increases to 10 min, these grains grow up, and the adjacent grains begin to splice. Meanwhile, grains stop growing at line 1 and line 2. The inserted AFM image in Figure 2b reveals that the growth stops at the edge of the steps. When the growth time reaches 15 min, the grains complete stitching and form a nanoribbon. Therefore, MoS₂ nanoribbons are not grown from a single grain but are formed through the stitching of multiple grains.

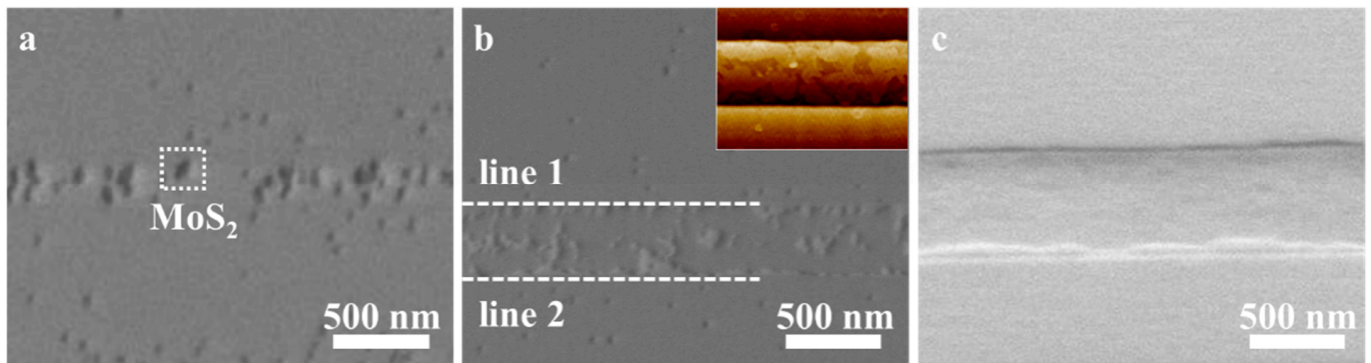


Figure 2. Evolution of morphology of MoS₂ nanoribbons with growth time. SEM images for 5 min (a), 10 min (b) with an inset of the corresponding AFM image, and 15 min (c).

To verify the orientation of the grains and the associated crystallinity of the MoS₂ nanoribbons, the samples were characterized with TEM and SHG. Figure 3a shows the transferred nanoribbons, marked with two dashed lines. A HRTEM image of a nanoribbon (Figure 3b) reveals clear light/dark contrast, enabling the identification of Mo and S atoms. The crystal displays a near-perfect atomic lattice, indicative of high crystallinity. Furthermore, the high crystallinity of the triangle crystal is also revealed in Figure S2, which confirms that the step height does not influence the quality of MoS₂. The SAED pattern of a nanoribbon is shown in Figure 3c, and the MoS₂ grains exhibit one set of hexagonal diffraction spots. We compared the diffraction spot angles in 150 regions and found that the angles were consistent (Figure 3d), which reveals that the grains possess a highly aligned orientation. However, MoS₂ crystals belong to space group *p63/mmc*, meaning that the diffraction spots of the 0° and 60° orientations are equivalent. We cannot recognize the differences between these two types crystals via SAED. Grains stitched by different orientations would produce grain boundaries [26,27]. When monolayer MoS₂ crystals are stitched with a misorientation of 60°, a 4|4E-type grain boundary forms. The SHG signal is quenched at this type of grain boundary, making it detectable via intensity mapping [28]. The SHG mapping (Figure 3e) of a nanoribbon exhibits a uniform intensity distribution, indicating the absence of 4|4E-type grain boundaries. Therefore, all grains share the same orientation, and the stitched MoS₂ nanoribbons are monocrystalline.

To better understand the different growth behaviors of the two surfaces, CP2K calculations were further conducted. Firstly, we calculated the difference in binding energy, whereas the binding energy of MoS₂ on a flat surface is set as the energy reference. As shown in Figure 4a, the binding energy difference changes from −1.79 eV for a 1.54 nm-high step to −1.86 eV for a 1.98 nm-high step, suggesting that, energetically, the MoS₂ domain prefers to nucleate at higher steps. Second, the “step-climbing” energy barriers were calculated to be 8.48 eV and 8.61 eV for a 1.54 nm-high step and a 1.98 nm-high step (Figure 4b), which indicates that climbing across a higher step is more difficult. Moreover, the calculation for a 0.66 nm-high step confirms this conclusion, as shown in Figure S3.

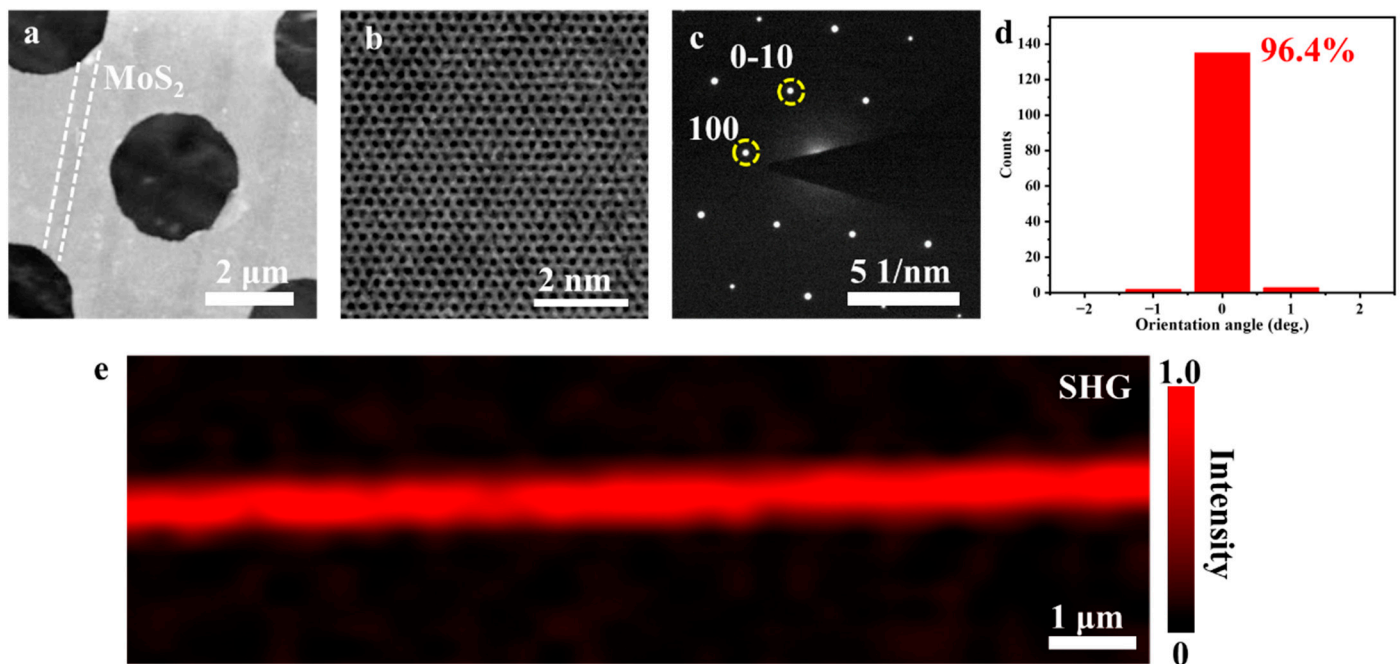


Figure 3. The crystallinity of MoS₂ grains of nanoribbons. (a) Low-magnification TEM image of nanoribbons and corresponding high-resolution TEM image (b) of SAED pattern (c). The (0–10) crystal plane in (c) is defined as the x-direction, and thus the orientation angle in (d) is defined as the angle between the (0–10) crystal plane and the x-direction. (e) SHG mapping of a MoS₂ nanoribbon.

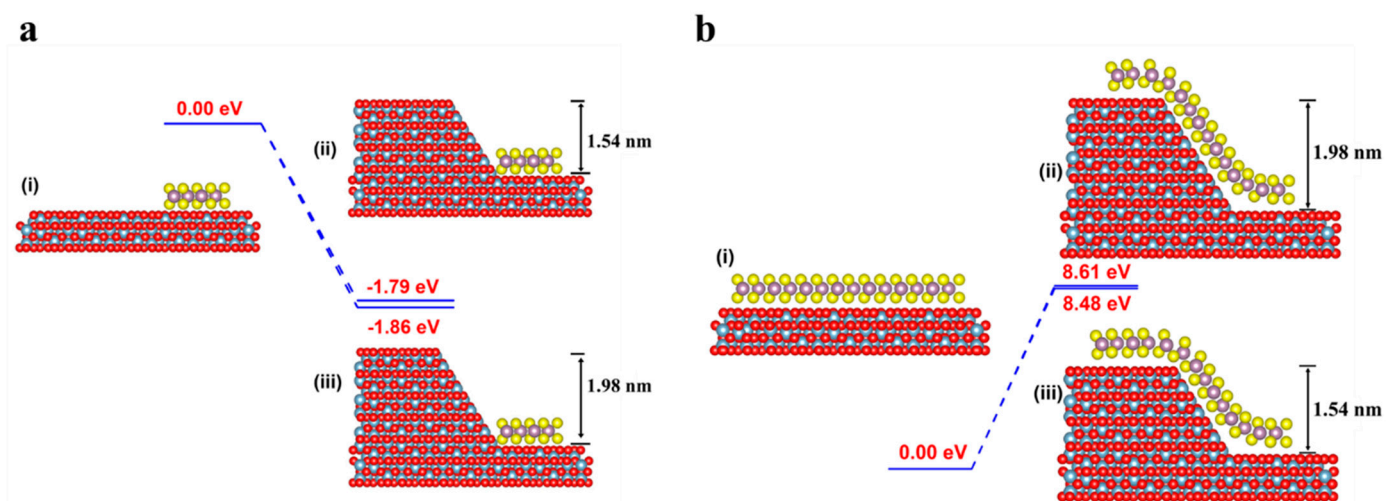


Figure 4. CP2K calculations of the growth. (a) Energy profiles of MoS₂ on a flat surface (i) attached to a 1.54 nm-high step (ii) and a 1.98 nm-high step (iii). (b) Energy profiles of MoS₂ on a flat surface (i) crossing a 1.54 nm-high step (ii) and a 1.98 nm-high step (iii), respectively. The binding energies of MoS₂ on a flat surface are set as energy references.

Based on the above-mentioned results, we proposed the following mechanism for the growth of MoS₂ on the LSS and HSS. Firstly, due to the lower nucleation energy at the step edge and the design of the step direction, highly oriented crystals are formed at the step edge on both substrates, as shown in Figure 5a,d. With an increasing deposition time, the grains continue to grow. Since the energy required to cross the step on the surface of the LSS is relatively low, the sample exhibits cross-step growth (Figure 5b,c). However, the energy required for crossing the step is too high on the HSS. Hence, as shown in Figure 5e, the crystals nucleating at the same step edge cannot cross the step (i.e., grow within the step surface). Eventually, it forms nanoribbons in the same direction as the step (Figure 5f).

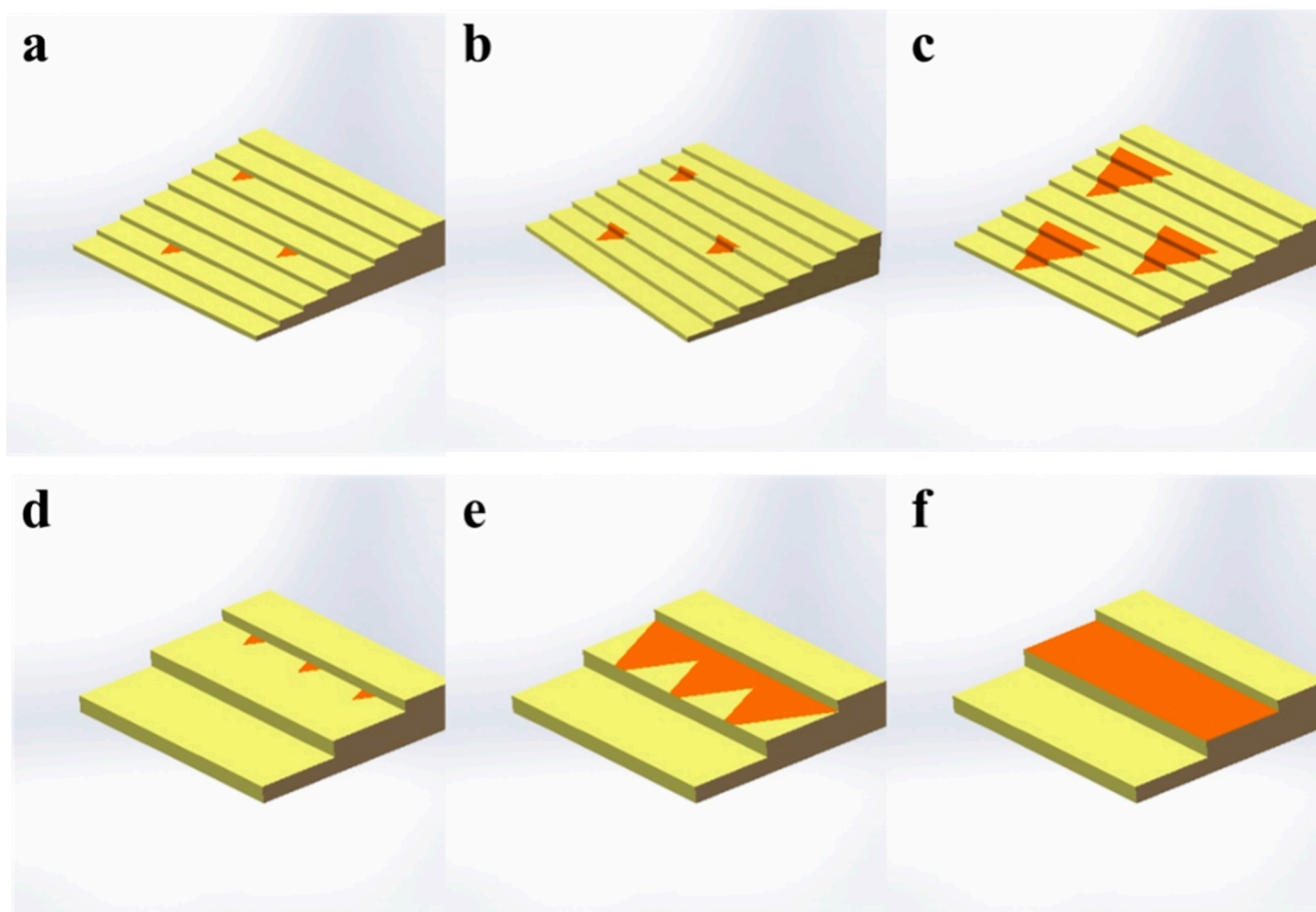


Figure 5. The schematic diagram for the growth of monolayer MoS₂. Growth on LSS (a–c) and HSS (d–f).

4. Conclusions

In summary, we demonstrated the effect of the step height of the sapphire substrate on the growth of monolayer MoS₂. Triangular crystals with a consistent orientation were prepared on an LSS, while unidirectional nanoribbons were obtained on a HSS. The nanoribbon was formed by multiple grains and proved to be a single crystal. Step height did not influence the quality of the MoS₂. The CP2K calculations revealed the promotion of nucleation and the inhibition of cross-step growth with larger step heights. The results shed light on the growth mechanism of monolayer MoS₂ and could promote its applications in electrical, optical, and energy-related devices.

Supplementary Materials: The following supporting information can be downloaded at <https://www.mdpi.com/article/10.3390/nano13233056/s1>: Figure S1: PL spectra of MoS₂ with triangle (a) and nanoribbon (b); Figure S2: the crystallinity of triangle MoS₂; Figure S3: CP2K calculations about the growth.

Author Contributions: Conceptualization, J.L. (Jie Lu) and M.Z.; methodology, J.L. (Jinxin Liu); writing—original draft preparation, J.L. (Jie Lu) and M.Z.; writing—review and editing, Y.Z.; supervision, W.C.; funding acquisition, X.Z. and Y.Z. All authors have read and agreed to the published version of the manuscript.

Funding: The authors appreciate the financial support from the National Natural Science Foundation of China (Grant No. 12374193 and Grant No. 12174321).

Institutional Review Board Statement: Not applicable.

Informed Consent Statement: Not applicable.

Data Availability Statement: The data presented in this study are available from the corresponding author upon reasonable request.

Conflicts of Interest: The authors declare no conflict of interest.

References

1. Li, W.S.; Gong, X.S.; Yu, Z.H.; Ma, L.; Sun, W.J.; Gao, S.; Köroglu, Ç.; Wang, W.F.; Liu, L.; Li, T.T.; et al. Approaching the Quantum Limit in Two-Dimensional Semiconductor Contacts. *Nature* **2023**, *613*, 274–279. [[CrossRef](#)] [[PubMed](#)]
2. Feng, S.; Liu, C.; Zhu, Q.B.; Su, X.; Qian, W.W.; Sun, Y.; Wang, C.X.; Li, B.; Chen, M.L.; Chen, L.; et al. An Ultrasensitive Molybdenum-Based Double-Heterojunction Phototransistor. *Nat. Commun.* **2021**, *12*, 4094. [[CrossRef](#)] [[PubMed](#)]
3. Sun, Y.X.; Jiang, L.Y.; Wang, Z.; Hou, Z.F.; Dai, L.Y.; Wang, Y.K.; Zhao, J.Y.; Xie, Y.H.; Zhao, L.B.; Jiang, Z.D.; et al. Multiwavelength High-Detectivity MoS₂ Photodetectors with Schottky Contacts. *ACS Nano* **2022**, *16*, 20272–20280. [[CrossRef](#)] [[PubMed](#)]
4. Wang, Z.; Kang, Y.; Hu, J.; Ji, Q.; Lu, Z.; Xu, G.; Qi, Y.; Zhang, M.; Zhang, W.; Huang, R.; et al. Boosting CO₂ Hydrogenation to Formate over Edge-Sulfur Vacancies of Molybdenum Disulfide. *Angew. Chem. Int. Ed.* **2023**, *62*, e202307086. [[CrossRef](#)] [[PubMed](#)]
5. Sangiovanni, D.G.; Faccio, R.; Gueorguiev, G.K.; Kakanakova-Georgieva, A. Discovering Atomistic Pathways for Supply of Metal Atoms from Methyl-Based Precursors to Graphene Surface. *Phys. Chem. Chem. Phys.* **2023**, *25*, 829–837. [[CrossRef](#)] [[PubMed](#)]
6. Kakanakova-Georgieva, A.; Ivanov, I.G.; Suwannaharn, N.; Hsu, C.W.; Cora, I.; Pécz, B.; Giannazzo, F.; Sangiovanni, D.G.; Gueorguiev, G.K. MOCVD of AlN on Epitaxial Graphene at Extreme Temperatures. *CrystEngComm* **2021**, *23*, 385–390. [[CrossRef](#)]
7. Al Balushi, Z.Y.; Wang, K.; Ghosh, R.K.; Vilá, R.A.; Eichfeld, S.M.; Caldwell, J.D.; Qin, X.Y.; Lin, Y.C.; DeSario, P.A.; Stone, G.; et al. Two-Dimensional Gallium Nitride Realized Via Graphene Encapsulation. *Nat. Mater.* **2016**, *15*, 1166–1171. [[CrossRef](#)]
8. Yang, P.F.; Zou, X.L.; Zhang, Z.P.; Hong, M.; Shi, J.P.; Chen, S.L.; Shu, J.P.; Zhao, L.Y.; Jiang, S.L.; Zhou, X.B.; et al. Batch Production of 6-Inch Uniform Monolayer Molybdenum Disulfide Catalyzed by Sodium in Glass. *Nat. Commun.* **2018**, *9*, 979. [[CrossRef](#)]
9. Zhou, J.D.; Lin, J.H.; Huang, X.W.; Zhou, Y.; Chen, Y.; Xia, J.; Wang, H.; Xie, Y.; Yu, H.M.; Lei, J.C.; et al. A Library of Atomically Thin Metal Chalcogenides. *Nature* **2018**, *556*, 355–359. [[CrossRef](#)]
10. Yu, H.; Liao, M.; Zhao, W.; Liu, G.; Zhou, X.J.; Wei, Z.; Xu, X.; Liu, K.; Hu, Z.; Deng, K.; et al. Wafer-Scale Growth and Transfer of Highly-Oriented Monolayer MoS₂ Continuous Films. *ACS Nano* **2017**, *11*, 12001–12007. [[CrossRef](#)]
11. Zhang, K.A.; She, Y.H.; Cai, X.B.; Zhao, M.; Liu, Z.J.; Ding, C.C.; Zhang, L.J.; Zhou, W.; Ma, J.H.; Liu, H.W.; et al. Epitaxial Substitution of Metal Iodides for Low-Temperature Growth of Two-Dimensional Metal Chalcogenides. *Nat. Nanotechnol.* **2023**, *18*, 448–455. [[CrossRef](#)] [[PubMed](#)]
12. Yang, P.; Zhang, S.; Pan, S.; Tang, B.; Liang, Y.; Zhao, X.; Zhang, Z.; Shi, J.; Huan, Y.; Shi, Y.; et al. Epitaxial Growth of Centimeter-Scale Single-Crystal MoS₂ Monolayer on Au(111). *ACS Nano* **2020**, *14*, 5036–5045. [[CrossRef](#)] [[PubMed](#)]
13. Li, T.T.; Guo, W.; Ma, L.; Li, W.S.; Yu, Z.H.; Han, Z.; Gao, S.; Liu, L.; Fan, D.X.; Wang, Z.X.; et al. Epitaxial Growth of Wafer-Scale Molybdenum Disulfide Semiconductor Single Crystals on Sapphire. *Nat. Nanotechnol.* **2021**, *16*, 1201–1207. [[CrossRef](#)]
14. Wang, J.; Xu, X.; Cheng, T.; Gu, L.; Qiao, R.; Liang, Z.; Ding, D.; Hong, H.; Zheng, P.; Zhang, Z.; et al. Dual-Coupling-Guided Epitaxial Growth of Wafer-Scale Single-Crystal WS₂ Monolayer on Vicinal a-Plane Sapphire. *Nat. Nanotechnol.* **2021**, *17*, 33–38. [[CrossRef](#)] [[PubMed](#)]
15. Zheng, P.M.; Wei, W.Y.; Liang, Z.H.; Qin, B.; Tian, J.P.; Wang, J.H.; Qiao, R.X.; Ren, Y.L.; Chen, J.T.; Huang, C.; et al. Universal Epitaxy of Non-Centrosymmetric Two-Dimensional Single-Crystal Metal Dichalcogenides. *Nat. Commun.* **2023**, *14*, 592. [[CrossRef](#)]
16. Liu, L.; Li, T.T.; Ma, L.; Li, W.S.; Gao, S.; Sun, W.J.; Dong, R.K.; Zou, X.L.; Fan, D.X.; Shao, L.W.; et al. Uniform Nucleation and Epitaxy of Bilayer Molybdenum Disulfide on Sapphire. *Nature* **2022**, *605*, 69–75. [[CrossRef](#)]
17. Dong, R.K.; Gong, X.S.; Yang, J.F.; Sun, Y.M.; Ma, L.; Wang, J.L. The Intrinsic Thermodynamic Difficulty and a Step-Guided Mechanism for the Epitaxial Growth of Uniform Multilayer MoS₂ with Controllable Thickness. *Adv. Mater.* **2022**, *34*, e2201402. [[CrossRef](#)]
18. Kühne, T.D.; Iannuzzi, M.; Del Ben, M.; Rybkin, V.V.; Seewald, P.; Stein, F.; Laino, T.; Khaliullin, R.Z.; Schütt, O.; Schiffmann, F.; et al. CP2K: An Electronic Structure and Molecular Dynamics Software Package—Quickstep: Efficient and Accurate Electronic Structure Calculations. *J. Chem. Phys.* **2020**, *152*, 194103. [[CrossRef](#)]
19. VandeVondele, J.; Krack, M.; Mohamed, F.; Parrinello, M.; Chassaing, T.; Hutter, J. Quickstep: Fast and Accurate Density Functional Calculations Using a Mixed Gaussian and Plane Waves Approach. *Comput. Phys. Commun.* **2005**, *167*, 103–128. [[CrossRef](#)]
20. VandeVondele, J.; Hutter, J. Gaussian Basis Sets for Accurate Calculations on Molecular Systems in Gas and Condensed Phases. *J. Chem. Phys.* **2007**, *127*, 114105. [[CrossRef](#)]
21. Krack, M. Pseudopotentials for H to Kr Optimized for Gradient-Corrected Exchange-Correlation Functionals. *Theor. Chem. Acc.* **2005**, *114*, 145–152. [[CrossRef](#)]
22. Hartwigsen, C.; Goedecker, S.; Hutter, J. Relativistic Separable Dual-Space Gaussian Pseudopotentials from H to Rn. *Phys. Rev. B* **1998**, *58*, 3641–3662. [[CrossRef](#)]
23. Perdew, J.P.; Burke, K.; Ernzerhof, M. Generalized Gradient Approximation Made Simple. *Phys. Rev. Lett.* **1996**, *77*, 3865–3868. [[CrossRef](#)] [[PubMed](#)]
24. Grimme, S.; Ehrlich, S.; Goerigk, L. Effect of the Damping Function in Dispersion Corrected Density Functional Theory. *J. Comput. Chem.* **2011**, *32*, 1456–1465. [[CrossRef](#)] [[PubMed](#)]

25. Lu, T.; Chen, F.W. Multiwfn: A Multifunctional Wavefunction Analyzer. *J. Comput. Chem.* **2012**, *33*, 580–592. [[CrossRef](#)] [[PubMed](#)]
26. Ji, H.G.; Lin, Y.C.; Nagashio, K.; Maruyama, M.; Solís-Fernández, P.; Aji, A.S.; Panchal, V.; Okada, S.; Suenaga, K.; Ago, H. Hydrogen-Assisted Epitaxial Growth of Monolayer Tungsten Disulfide and Seamless Grain Stitching. *Chem. Mater.* **2018**, *30*, 403–411. [[CrossRef](#)]
27. Ago, H.; Fukamachi, S.; Endo, H.; Solís-Fernández, P.; Yunus, R.M.; Uchida, Y.; Panchal, V.; Kazakova, O.; Tsuji, M. Visualization of Grain Structure and Boundaries of Polycrystalline Graphene and Two-Dimensional Materials by Epitaxial Growth of Transition Metal Dichalcogenides. *ACS Nano* **2016**, *10*, 3233–3240. [[CrossRef](#)]
28. Wang, Q.Q.; Li, N.; Tang, J.; Zhu, J.Q.; Zhang, Q.H.; Jia, Q.; Lu, Y.; Wei, Z.; Yu, H.; Zhao, Y.C.; et al. Wafer-Scale Highly Oriented Monolayer Mos2 with Large Domain Sizes. *Nano Lett.* **2020**, *20*, 7193–7199. [[CrossRef](#)]

Disclaimer/Publisher’s Note: The statements, opinions and data contained in all publications are solely those of the individual author(s) and contributor(s) and not of MDPI and/or the editor(s). MDPI and/or the editor(s) disclaim responsibility for any injury to people or property resulting from any ideas, methods, instructions or products referred to in the content.